Journal of Crystal Growth ∎ (∎∎∎∎) ∎∎∎–∎∎∎

Contents lists available at ScienceDirect

Journal of Crystal Growth

journal homepage: www.elsevier.com/locate/jcrysgro

Motion of equiaxed grains during directional solidification under static magnetic field

G. Salloum-Abou-Jaoude [a,b], J. Wang [c,d,e], L. Abou-Khalil [a,b], G. Reinhart [a,b], Z. Ren [c], N. Mangelinck-Noel [a,b], X. Li [c], Y. Fautrelle [d], Henri Nguyen-Thi [a,b,*]

[a] Aix Marseille University, Campus Saint-Jerome, Case 142, Marseille Cedex 20 13397, France
[b] CNRS, IM2NP, Campus Saint-Jerome, Case 142, Marseille Cedex 20 13397, France
[c] Department of Material Science and Engineering, Shanghai University, Shanghai 200072, PR China
[d] SIMAP/EPM, 1130 rue de la Piscine BP 75 ENSEEG, St-Martin d'Heres 38402, France
[e] School of Materials, The University of Manchester, Oxford Road, Manchester M13 9PL, UK

ARTICLE INFO

Keywords:
A1. Equiaxed grain motion
A1. Equiaxed growth
A1. Thermoelectric magnetic forces
A1. X-ray radiography
B1. Alloys
B1. Metals

ABSTRACT

The in situ and real time observations of the equiaxed grain motion during directional solidification of Al–10 wt% Cu under static magnetic field has been carried out by means of synchrotron X-ray radiography. It was observed that equiaxed grains moved approximately along the direction perpendicular to both the imposed magnetic field and the temperature gradient. Based on the radiographs, the motion of the solid grains was analyzed for various temperature gradients, and it was shown that the trajectories were imposed by the combination of the Thermo-Electric Magnetic forces, induced by the coupling of thermo-electric currents with the permanent magnetic field and the gravity force. The variations of the velocities and sizes of grains during the equiaxed growth under static magnetic field were measured and compared to a simple analytical model for the Thermo-Electric Magnetic forces and the Stokes law. A good agreement was achieved for the deviation angle as a function of the grain diameter, while a large discrepancy was observed for the velocity intensity when the dimensions of the equiaxed grains increased. In the latter case, it was shown that the corrections for both sample confinement and grain morphology were mandatory to explain the very low values of grain velocities.

1. Introduction

The use of external magnetic fields is a widespread technique to control the flows in the melt during metal solidification and then to modify the final properties of the grown material, leading to improvement of the process performance and better quality products [1–3]. The main advantage of this technique is to be contactless, which prevent alloy contamination, and also to avoid any risk when using brittle crucible. A non-permanent magnetic field may be utilized to increase melt stirring, which may be useful for producing either a more uniform melt by a strong mixing in the liquid phase, or a shear flow to induce grain refinement effects during metal casting. Alternatively, a permanent magnetic field can be used in order to damp or eliminate convection during solidification due to the Lorentz force, generated by the interaction between the induced electric current and the applied magnetic field [4,5]. It is well recognized that electromagnetic braking reduces inclusions and improved uniformity of compositions and mechanical properties. In addition, Shercliff [6] pointed out that a static magnetic field can produce flows in melt during the metallurgy process caused by the interaction of the magnetic field with variations of the Seebeck coefficients at the solid–liquid interface. Such flows have been well studied in the case of solidification of metallic alloys [7–9] and in the context of pumping or stirring liquid metal coolants in nuclear reactor [10].

Another important but neglected aspect up to now is the existence of the Thermo-Electro-Magnetic Forces (TEMF), created by the interaction between the electric current generated by the thermoelectric effect in the vicinity of the liquid–solid interface submitted to a temperature gradient (Thomson–Seebeck effect) and the static magnetic field [6,8]:

$$F_{TEM} = j \times B_0 \quad (1)$$

* Corresponding author at: Aix-Marseille University, IM2NP, Campus St-Jerome, Case 142, Avenue Escadrille Normandie-Niemen, 13397 Marseille France. Tel.: +33 491282893; fax: +33 491288775.
E-mail address: henri.nguyen-thi@im2np.fr (H. Nguyen-Thi).

http://dx.doi.org/10.1016/j.jcrysgro.2014.10.058
0022-0248/

where F_{TEM} stands for the Thermo-Electro-Magnetic force (TEMF), j the electric current and B_0 the applied static magnetic field. Thermo-electric currents in each phase are generated by a temperature difference along the solid–liquid interface and are function of the solid and liquid phase Seebeck coefficients (S_l and S_s) and the temperature gradient $G=\nabla T$. Then the electric current density in each phase may be written as follows:

$$j_i = -\sigma_i(\nabla V + S_i \nabla T),\ i = l, s \ \text{respectively in the liquid and in the solid.} \tag{2}$$

In Eq. (2) V denotes the electric scalar potential and σ_i the electrical conductivity of solid or liquid phase. The second term of the right hand side in Eq. (2) accounts for the contribution of the thermoelectric current via the thermoelectric power S_i of the materials. The electric current created by the interaction between the fluid motion and the applied magnetic field, which is given by $\sigma_l(u \times B)$, is neglected in Eq. (2). In fact, the influence of that contribution to the total electric current density is quantified by the Hartmann number, $Ha = B_0 L\sqrt{\sigma_l/\mu}$, the ratio of the electromagnetic force to the viscous force [11], with μ the dynamic viscosity. Taking $L \approx 50$ μm, the typical dimension of the liquid flow around the solid grain, the value of Ha is around 0.2, which is lower than 10, the value over which braking is felt, and justifies the above approximation. Note that for large size grains there is a confinement of the electric current density in the liquid bath due to the presence of the lateral walls. The latter effect tends to decrease the electromagnetic force on the particle [12].

In a recent paper [13], it has been demonstrated using in situ observation by means of synchrotron X-ray radiography that TEMF forced the dendrite fragments to move roughly horizontally, instead of vertically downward as it is the case in solidification experiments without magnetic field. Actually, for Al–Cu alloys having a composition lower Al–10 wt% Cu, the solid grains are weakly denser than the surrounding melt and thus settle down in the liquid phase in the absence of magnetic field [14]. This observation is in qualitative agreement with the prediction of an analytical model assuming a spherical solid particle immersed in a liquid metal under an imposed constant vertical thermal gradient, which shows that the TEMF acting on the particle has only one component along horizontal y-direction and its intensity is proportional to the volume Vol of the sphere [13]:

$$F_y = -2\left[\frac{\sigma_s\sigma_l}{2\sigma_l+\sigma_s}\right](S_s - S_l)\, G B_0 Vol \tag{3}$$

In the present paper, we describe experimental results on the effect of TEMF on the motion of equiaxed grains, formed during the solidification of an Al–10 wt% Cu sample. For this purpose and since these phenomena were in essence dynamic, it is of major interest to be able to investigate in situ and in real time the solidification process. As a consequence, synchrotron X-ray imaging was used, which has been established as a method of choice for such studies [15,16].

2. Experiments

The experiments were carried out on beamline BM05 at the European Synchrotron Radiation Facility (ESRF, Grenoble, France). Directional solidification experiments were performed inside a Bridgman furnace, which has been described in detail previously [17]. The thermal gradient G (along the z-direction) was imposed by two separated heating elements and the solidification was controlled by applying the same cooling rate R on the two heating elements. The temperature adjustment was monitored using two embedded K-type thermocouples, one at the top and other at the bottom on either side of the sample, 2 cm away from each other. A series of solidification experiments were carried out with the same cooling rate $R=2$ K/min, the same permanent magnetic field, and various temperature gradient G decreasing from 20 K/cm to nearly zero. The thin sample studied was 35 mm in length, 5 mm in width and 230 μm in thickness. To minimize grain sinking phenomena, solidifications were conducted on Al–10 wt% Cu alloy for which the grain density is weakly larger than the surrounding liquid [14].

The static magnetic field was generated by a cubic neodymium magnet (50 mm × 50 mm × 50 mm), which was fixed close to the Bridgman furnace and imposed a permanent magnetic field B_0 of 0.08 T. The direction of the field was set before the experiment parallel (x-direction) to the beam, and its intensity was almost uniform over the sample.

The solid–liquid interface was visualized by X-ray radiography: the main surface of the sample (y–z plane) was set perpendicular to the incident monochromatic X-ray beam. Absorption is the main source of the image contrast and mainly depends on the atomic number of the elements and the solute content. In our experiments, the X-ray energy was adjusted to 17.5 keV, which is an appropriate value for hypoeutectic Al–Cu alloys. In all the radiographic images, the aluminum solid microstructures appear in white and the copper-rich liquid in dark gray. The optics were chosen to obtain a large field of view (10 mm × 6 mm), which is essential in these kinds of studies to visualize and follow the motion of equiaxed grains over a long distance. The resolution was then imposed by the optics (pixel size 7.46 μm × 7.46 μm), which was sufficient for our purpose. The high intensity of synchrotron radiation makes it possible to record images with enough contrast in a reasonable timescale (~0.7 s), which is sufficient to investigate the movement of the equiaxed grains during solidification. The details of this synchrotron X-ray radiography setup can be found in Ref. [17].

To ease the grain motion analysis, a simple image processing was used, which consisted of taking the maximum intensity of successive radiographs to create a single image (Fig. 1). As the α-Al grains appeared in white in radiographs, this image processing revealed the successive positions of the grain and thus its trajectory (black dashed line with arrow in Fig. 1). Then, the time evolution of key parameters such as the grain surface, the velocity and the angle θ between the trajectory and the gravity direction can be easily measured. It is worth noticing that all the grains are not equivalent, because they nucleated at different instants along the experiment and then experienced different environment (number of neighbors, solute segregation in the sample). For this

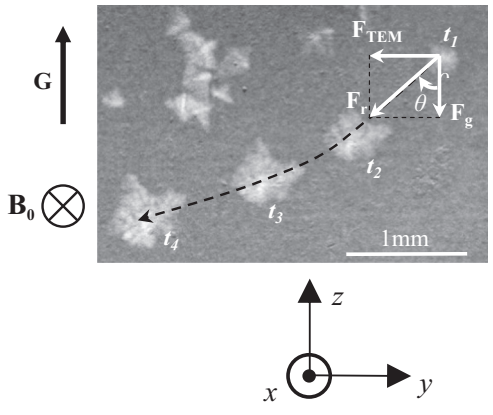

Fig. 1. Image showing the maximum intensity of four successive radiographs, revealing the four successive positions of a growing grain and thus its trajectory. The forces acting on the grain are indicated by the white arrows (F_g: the buoyancy force, F_{TEM}: the Thermo-Electro-Magnetic force and F_r: the resultant force). θ is the angle of the resultant force in respect to gravity.

Please cite this article as: G. Salloum-Abou-Jaoude, et al., Journal of Crystal Growth (2014), http://dx.doi.org/10.1016/j.jcrysgro.2014.10.058

reason, measurements on a limited number of grains were performed, on their very early stages of growth and when there is no apparent interaction with their neighboring grains. Despite these precautions, a large measurement deviation was generally observed and only a statistic analysis may be significant.

3. Results

3.1. Experimental evidence of the TEM force

Fig. 2 shows the time evolution of the solidification microstructure for a temperature gradient $G=10$ K/cm. The presence of an axial temperature gradient in the molten sample led to a non-homogeneous nucleation phase, from the bottom to the top of the sample. More specifically, first grains nucleated and showed up earlier in the cooler bottom part of the sample. As discussed in a previous paper [18], it can be reasonably assumed that the grain nucleation takes place from heterogeneous nucleation events at the crucible wall/oxide skin at liquidus temperature, or negligibly below. After the nucleation, few grains remained stuck on the oxide layer of the sample but the great majority of the grains moved roughly from the right side to the left side of the sample as indicated by few red arrows in Fig. 2a–d. It is worth noticing that the grains continued to grow during their motion. The global movement of the grains caused the equiaxed grains to form a tightly packed dendritic matrix on the left side of the sample which gradually moved towards the right side of the sample. This effect is more easily visible in the video (see Supplementary material), available on-line. Because grains were forced to move towards one side of the sample during the equiaxed growth, the number of grains across the transverse direction of the sample was non-uniform, as well as their size. It is worth noticing that such non-uniform microstructure could yield to non-uniform

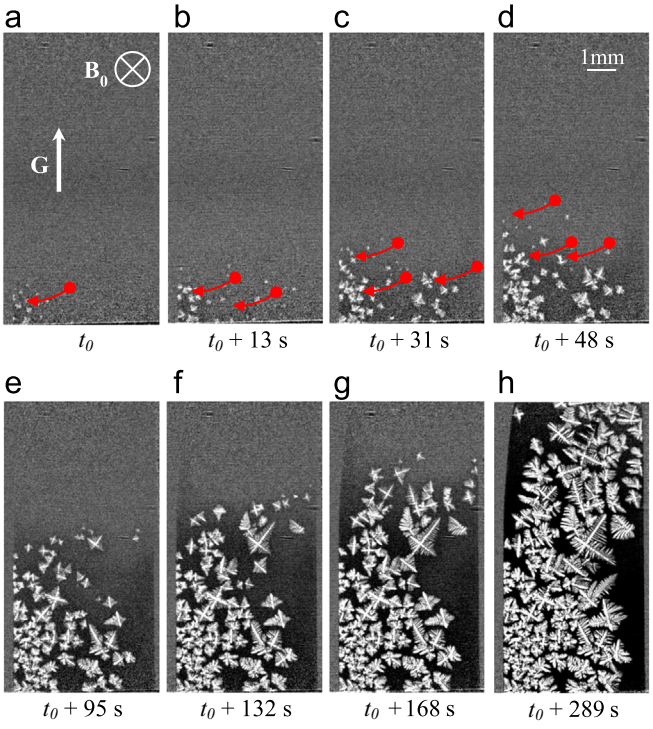

Fig. 2. Sequence of radiographs showing the equiaxed solidification experiment of Al–10 wt% Cu (cooling rate $R=2$ K/min; $G=10$ K/cm) under a 0.08 T static magnetic field. Equiaxed grains nucleated from the bottom to the top, according to the temperature gradient direction, and then moved from right to left in the sample as indicated by few red arrows in Fig. 2a–d. (For interpretation of the references to color in this figure legend, the reader is referred to the web version of this article.)

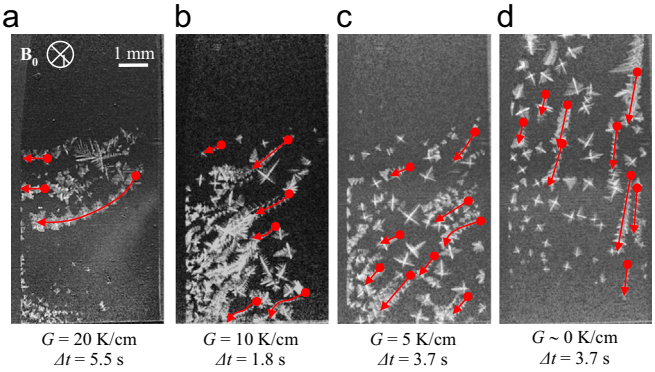

Fig. 3. Maximum exposure intensity of successive radiographs (Δt is the time interval between two successive radiographs) showing the equiaxed solidification experiments of Al–10 wt% Cu (cooling rate $R=2$ K/min) under a 0.08 T static magnetic field at different temperature gradients. The trajectories of few grains are represented by red arrows.

properties and chemical inhomogeneities, which may be detrimental for the final use of the grown material. The fact that all free grains moved from the right side toward the left side of the sample definitely demonstrates that the grains were pushed by a horizontal force in y-direction and not by any convection currents.

Supplementary material related to this article can be found online at http://dx.doi.org/10.1016/j.jcrysgro.2014.10.058.

In addition, the grain motion from the right side to the left side of the sample was observed in all the experiments with a non-zero temperature gradient as shown in Fig. 3, where some grain trajectories are drawn using the image processing described in the experimental section. It is already possible to see from this series of pictures that the effect decreases when the temperature decreases. Finally, when the temperature gradient was close to zero (Fig. 3d), the grains nucleated and then simply fell down almost vertically, due to gravity force. This dependence of the TEM force versus the temperature gradient is in agreement with Eq. (3), which suggests that the grains are forced to move horizontally by the Thermo-Electro-Magnetic force which acted on the grains.

3.2. Angle between the trajectory and the vertical direction in the early stages of growth

As qualitatively visible in Fig. 3, the angle between the mean trajectory of equiaxed grains and the gravity direction increased when the thermal gradient was increased from nearly zero to 20 K/cm. It is worth noticing that this angle does not depend on the grain dimensions, as both gravity force and TEM force are proportional to the grain volume. However, this angle can change during the grain motion due to the interaction between the grain and its environment, in particular with other stuck grains. Consequently, the determination of the angle θ between the trajectory and the gravity direction (Fig. 1) was determined for about 10 grains for each temperature gradient, only in the early stages of growth when they were assumed to be nearly isolated and relatively small compared to the sample thickness.

Fig. 4 shows the variation of the angle θ as a function of the temperature gradient G. The error bars were deduced from the multiple measurements for each value of G, and the plain line is calculated from

$$\tan\theta = \frac{-2\sigma_s\sigma_l(S_s-S_l)}{(2\sigma_l+\sigma_s)(\rho_s-\rho_l)g}GB_0 \quad (4)$$

Using the values given in Table 1, a very good agreement was found between experimental data and model predictions for this

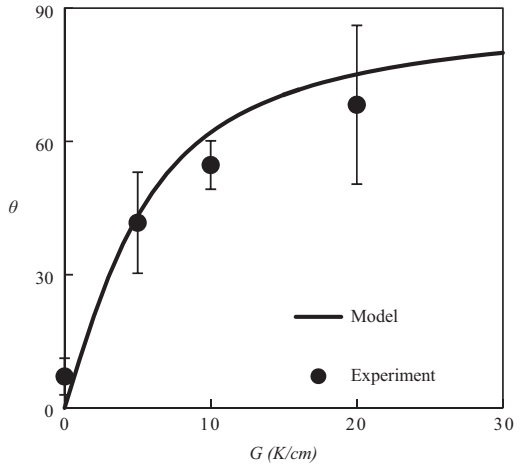

Fig. 4. Variation of the angle θ between the trajectory of the equiaxed grain and gravity direction. The plain line is the calculated angle and the symbols are the experimental values measured for each experiment at a temperature gradient G (G=0, 5, 10 and 20 K/cm). The error bar is the standard deviation over 10 grains for each experiment.

Table 1
Physical parameters used in the model calculation.

Physical parameter	Unit	Value
σ_S	$\Omega^{-1}\,m^{-1}$	10×10^{6}
σ_l	$\Omega^{-1}\,m^{-1}$	3.8×10^{6}
S_S	V K	-5.4×10^{-6}
S_l	V K	-3.8×10^{-6}
ρ_S	kg m^{-3}	2590
ρ_l	kg m^{-3}	2560
μ	Pa s	1.4×10^{-3}

range of temperature gradient, which confirms that the equiaxed grain motion is effectively controlled by TEM and gravity forces.

3.3. Analysis of grain velocity as a function of grain size

The next step of this work is the analysis of grain velocity as a function of grain size. As already pointed out, the grains continued to grow during their motion. Consequently, the measurements of the grain surface and the grain velocity were carried out at each step of the solidification experiments, between two successive radiographs. The shape of a dendritic grain is obviously very complex and far from a spherical solid in three-dimensions or a circle in two-dimensions. For a non-circular particle, several methods can be used to determine an equivalent diameter of an equiaxed grain, based on the projected area of the dendrite, on the envelope of the dendrite, or on the maximum circle which includes the dendrite. We chose to work with the projected area method, an approach usually used in Fluid Mechanics, since it requires less parameter measurements than the other two. More precisely, when considering the envelope of the dendrite or the maximum circle including the dendrite, it is necessary to estimate a weighted density for each grain envelope as a function of the liquid and solid fractions to be used in the buoyancy force calculation. This required the measurement or estimation of the liquid fraction of the grain envelope, which is not possible in our experiments at the moment.

The "equivalent surface diameter" d_S can be defined as the diameter of the disc that would have the same area as the projected image of the envelope of the irregular dendritic grain:

$$d_S = \sqrt{\frac{4S_{grain}}{\pi}} \tag{5}$$

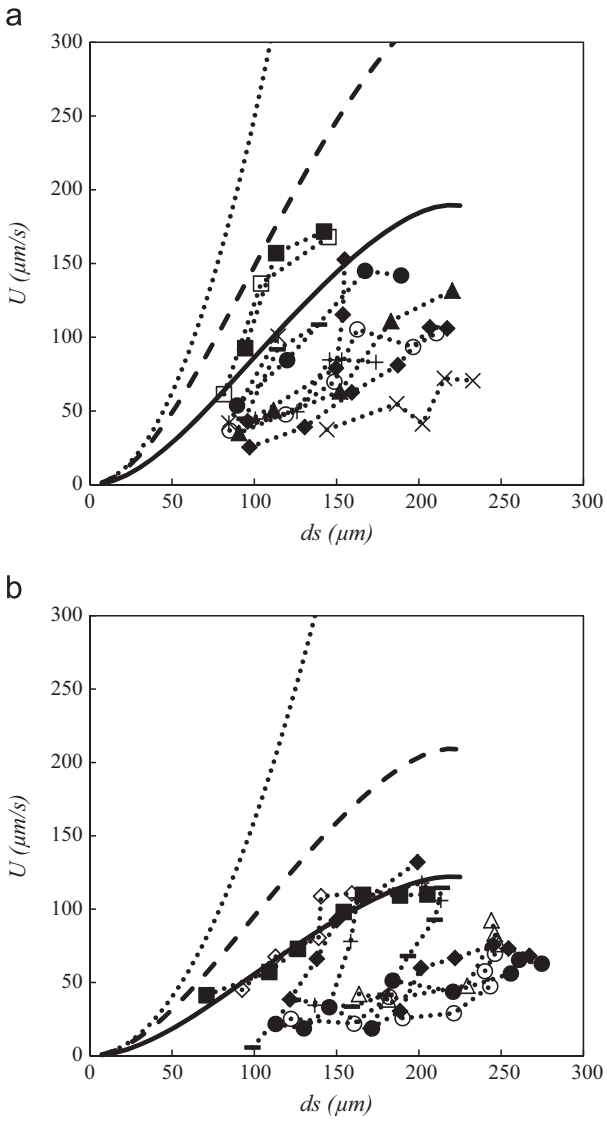

Fig. 5. Plot of the velocity as a function of the equiaxed grain diameter for a temperature gradient of (a) G=10 K/cm and (b) G=5 K/cm. The symbols represent experimental measurements of about 10 grains, nucleating almost at the same position in the sample. The Stokes model is indicated by the dotted line, the model with the wall correction to the Stokes model is plotted by a dashed line and the model taking into account both wall confinement and grain morphology is plotted in plain line.

This definition does not take into account phenomena which can take place in the third dimension (sample thickness direction), which will be discussed later in the paper. Fig. 5 shows the evolution of the grain velocity U for up to 10 grains as a function of the "equivalent surface diameter" d_S for two temperature gradients. The experimental points joined by a dotted line correspond to measurements performed on a single grain during its growth as a function of time. The grains were selected in the same area of the sample to prevent as possible any influence of sample thickness, temperature gradient or solute segregation. It is worth noticing that some of these grains nucleated exactly at the same position. Actually, as soon as the first grain moved freeing the heterogeneous nucleation site, a second one nucleated exactly at this position forming a chain of equiaxed grains. Despite these precautions, a large dispersion was observed for each value of diameter, which suggested that the grain history (nucleation and growth) has a strong impact on the grain velocity and only a statistical analysis is relevant in experiments.

In our experiments, the maximum Reynolds number $Re=Ud_S\rho_l/\mu$ (with μ the dynamic viscosity) is much lower than unity, typically

Please cite this article as: G. Salloum-Abou-Jaoude, et al., Journal of Crystal Growth (2014), http://dx.doi.org/10.1016/j.jcrysgro.2014.10.058

about 10^{-2}. Therefore in a first approximation we might assume to be in Stokes' regime and the velocity U can be deduced from the analytical expression of the TEM force (Eq. 3) and the gravity force:

$$U_{Stokes} = \frac{{d_S}^2}{18\mu}\sqrt{((\rho_S - \rho_L)g)^2 + \left(2\frac{\sigma_s\sigma_l(S_S - S_l)}{(2\sigma_l + \sigma_s)}GB_0\right)^2} \quad (6)$$

A comparison of the Stokes velocity (dot lines in Fig. 5a and b) with experimental data showed a large discrepancy: For the smallest diameter (about 80 μm) the Stokes velocity is already three times larger than the experimental values. Moreover, the discrepancy increases with the grain diameter d_S, which definitely rules out the use of the simple Stokes velocity in our experiments and suggests an increase of wall confinement.

The first improvement for the Stokes velocity is the correction for wall interference. Actually, it is well known that the motion of a sphere in a viscous fluid is dramatically slowed down in the presence of walls [19]. In a recent paper [20], the equiaxed dendritic growth in grain refined Al–Cu alloys has been studied in situ during directional solidification by means of synchrotron X-ray video microscopy, in a very similar experimental configuration. The authors derived a model based on the first approximation of the H. Faxén equation [21] for one spherical grain taking into account the influence of sample confinement on the drag force exerted on the free grain. They concluded that, as expected, confinement significantly slows down the grain velocity. In the present work, we take into consideration the original correction factor as presented by H. Faxén in 1922 [21]. This equation corresponds to our case when the grains settle in a liquid pool bounded by two parallel planes and is more precise. This will give the following expression of the settling velocity with respect to the blockage ratio (d_S/e), with e the sample thickness:

$$U_{confined} = U_{Stokes}\left[1 - 1.004\left(\frac{d_s}{e}\right) + 0.418\left(\frac{d_s}{e}\right)^3 - 0.169\left(\frac{d_s}{e}\right)^5\right] \quad (7)$$

Using this correction, the discrepancy between our experimental measurements and the predicted velocity is reduced as shown in Fig. 5a and b (dashed lines) but still remains large. It is must noticed that the presence of the electrically insulating walls causes an additional confinement effect of the electric current distribution around the particle. The latter confinement leads to a decrease of the TEM force acting on the particle [12]. It is worth noticing that, since nucleation occurs on the wall in our experiments, the assumption that the grain moves along the centerline of the sample may be wrong in particular in the early stages of growth and the drag force must be modified accordingly. We note that we stopped the calculation for the theoretical model at a value $d_s/e = 1$ corresponding to an equiaxed grain having an equivalent diameter equal to the thickness of the sample (≈ 230 μm). Beyond this value, the correction for the wall effect cannot be applied. For the sake of completeness measurements for $d_s > 230$ μm are shown in Fig. 5, since the grains continued to move and grow laterally in the sample projection plane even after reaching a size of the order of the sample thickness.

A second correction to the equiaxed grain velocity is possible by taken into account the effects of grain geometry on the drag force. Indeed, the complex dendritic shape of the grain must be considered as pointed out by Zakhem et al. [22]. Moreover, we could expect that the dendritic grain velocity depends on its orientation with respect to the motion direction. By an experimental study of low Reynolds number drag on laboratory models of dendrite fragments, they determined the ratio of the test object velocity U_{object} on the Stokes velocity:

$$KS = \frac{U_{object}}{U_{Stokes}} \quad (8)$$

Following their observations, the object velocity is always lower than the Stokes velocity, with KS varying in between 0.6 and 0.8, depending of the object shape. Using the speed ratio $KS \approx 0.6$ of an equiaxed grain shaped object, the predicted velocity is now much closer to experimental velocities (plain lines in Fig. 5a and b), which suggests that additional effects have to be considered, for instance electric current distribution for a non-spherical equiaxed grain, tilting or rotation of the grains during their motion, the grain–grain interaction or localized Thermo-Electro-Magnetic flows around grains [5], which are not considered in this paper. In addition, the two contributions (wall confinement and grain morphology) were applied successively but non-linear coupling could not be ruled out.

4. Conclusion

This work provides in situ and real time observations of equiaxed grain motion during directional solidification of Al–10 wt% Cu alloy under a weak static magnetic field (0.08 T). The experimental results show that equiaxed grains were moved approximately along a direction perpendicular to both the temperature gradient and the magnetic field direction, which confirms that the grains are forced to move by gravity force and TEM force. The deviation angle in the early stages of growth for the different temperature gradients was determined and compared to the prediction achieved by using an analytical model for a spherical particle. A good agreement was obtained. The variation of the grain velocity as a function of the grains diameter was then measured from the radiographs and compared with predictions of analytical models which partly take into the account the wall confinement and the grain morphology. The discrepancy may be explained by two reasons. Firstly, the drag force in our experiments is larger, possibly due to grain behavior (tilting and rotation) during the motion, long-distance interaction with other equiaxed grains, electromagnetically driven flow around the particle and local variation of liquid composition related to solute rejection during solidification. The second reason comes from the influence of both confinement and grain morphology on the electric current distribution which modify the TEM forces acting on the grain. In order to deepen our analysis, 3D simulations of TEM forces in both liquid and solid phases as well as TEM flows in liquid are required respectively for the sphere particle and the equiaxed grain case. This work is in progress.

Acknowledgments

We acknowledge T. Lafford (ESRF, BM05) for her help during experiments. This study was partly supported by the CNRS/ANR OPTIMAG Project (ANR-09-BLAN-0382), the National 973 Project (No. 2011CB610404), the Shanghai Committee of Science and Technology (No. 13521101102), the XRMON project (AO-2004-046) of the MAP program of the European Space Agency (ESA) and by the French National Space Agency (CNES No. 130615).

References

[1] D.T.J. Hurle, R.W. Series, Use of a Magnetic Field in Melt Growth, North Holland, Amsterdam, 1994.
[2] P. Rudolph, Travelling magnetic fields applied to bulk crystal growth from the melt: the step from basic research to industrial scale, J. Cryst. Growth 310 (2008) 1298–1306.
[3] P.A. Davidson, Magnetohydrodynamics in materials processing, Annu. Rev. Fluid Mech. 31 (1999) 273–300.
[4] R. Moreau, Magnetohydrodynamics, Kluwer Publications, Dordrecht, The Netherlands, 1990.
[5] J. Wang, Y. Fautrelle, Z.M. Ren, H. Nguyen-Thi, G.S. Abou Jaoude, G. Reinhart, N. Mangelinck-Noel, X. Li, I. Kaldre, Thermoelectric magnetic flows in melt during directional solidification, Appl. Phys. Lett. 104 (2014) 121916.

Please cite this article as: G. Salloum-Abou-Jaoude, et al., Journal of Crystal Growth (2014), http://dx.doi.org/10.1016/j.jcrysgro.2014.10.058

[6] J.A. Shercliff, Thermoelectric Magnetohydrodynamics, J. Fluid Mech. 91 (1979) 231–251.
[7] P. Dold, F.R. Szofran, K.W. Benz, Thermoelectromagnetic convection in vertical Bridgman grown germanium–silicon, J. Cryst. Growth 291 (2006) 1–7.
[8] P. Lehmann, R. Moreau, D. Camel, R. Bolcato, Modification of interdendritic convection in directional solidification by a uniform magnetic field, Acta Mater. 46 (1998) 4067–4079.
[9] X. Li, A. Gagnoud, Z. Ren, Y. Fautrelle, R. Moreau, Investigation of thermo-electric magnetic convection and its effect on solidification structure during directional solidification under a low axial magnetic field, Acta Mater. 57 (2009) 2180–2197.
[10] M.A. Jaworski, T.K. Gray, M. Antonelli, J.J. Kim, C.Y. Lau, M.B. Lee, M.J. Neumann, W. Xu, D.N. Ruzic, Thermoelectric magnetohydrodynamic stirring of liquid metals, Phys. Rev. Lett. 104 (2010) 094503.
[11] X. Li, Y. Fautrelle, Z. Ren, Influence of thermoelectric effects on the solid–liquid interface shape and cellular morphology in the mushy zone during the directional solidification of Al–Cu alloys under a magnetic field, Acta Mater. 55 (2007) 3803–3813.
[12] J. Wang, Etude de l'effet thermoélectrique magnétique en solidification directionnelle d'alliages Al–Cu, Grenoble University, Grenoble, 2013.
[13] J. Wang, Y. Fautrelle, Z.M. Ren, X. Li, H. Nguyen-Thi, N. Mangelinck-Noel, G. S. Abou Jaoude, Y.B. Zhong, I. Kaldre, A. Bojarevics, L. Buligins, Thermoelectric magnetic force acting on the solid during directional solidification under a static magnetic field, Appl. Phys. Lett. 101 (2012) 251904.
[14] H. Nguyen-Thi, A. Bogno, G. Reinhart, B. Billia, R.H. Mathiesen, G. Zimmermann, Y. Houltz, K. Löth, D. Voss, A. Verga, F.d. Pascale, Investigation of gravity effects on solidification of binary alloys with in situ X-ray radiography on earth and in microgravity environment, J. Phys.: Conf. Ser. 327 (2011) 012012.
[15] H. Nguyen-Thi, L. Salvo, R.H. Mathiesen, L. Arnberg, B. Billia, M. Suery, G. Reinhart, On the interest of synchrotron X-ray imaging for the study of solidification in metallic alloys, C.R. Phys. 13 (2012) 237–245.
[16] R.H. Mathiesen, L. Arnberg, H. Nguyen-Thi, B. Billia, In situ X-ray video microscopy as a tool in solidification science, JOM 64 (2012) 76–82.
[17] T. Schenk, H. Nguyen Thi, J. Gastaldi, G. Reinhart, V. Cristiglio, N. Mangelinck-Noël, H. Klein, J. Härtwig, B. Grushko, B. Billia, J Baruchel, Application of synchrotron X-ray imaging to the study of directional solidification of aluminium-based alloys, J. Cryst. Growth 275 (2005) 201–208.
[18] A. Bogno, H. Nguyen-Thi, G. Reinhart, B. Billia, J. Baruchel, Growth and interaction of dendritic equiaxed grains: in situ characterization by synchro-tron X-ray radiography, Acta Mater. 61 (2013) 1303–1315.
[19] E.R. Lindgren, The motion of a sphere in an incompressible viscous fluid at Reynolds numbers considerably less than one, Phys. Scr. 60 (1999) 97–110.
[20] P. Delaleau, R.H. Mathiesen, P.L. Schaffer, L. Arnberg, C. Beckermann, Modeling and in-situ X-Ray Video Microscopy of Confined Equiaxed Grain Growth and Buoyant Motion in Al–Cu, Minerals, Metals & Materials Soc., Warrendale, 2009.
[21] H. Faxén, The resistance against the movement of a rigour sphere in viscous fluids, which is embedded between two parallel layered barriers, Ann. der Phys. 373 (1922) 89–119.
[22] R. Zakhem, P.D. Weidman, H.C. Degroh, On the drag of model dendrite fragments at low Reynolds-number, Metall. Trans. A: Phys. Metall. Mater. Sci. 23 (1992) 2169–2181.

Please cite this article as: G. Salloum-Abou-Jaoude, et al., Journal of Crystal Growth (2014), http://dx.doi.org/10.1016/j.jcrysgro.2014.10.058